Hindawi
Shock and Vibration
Volume 2018, Article ID 2862143, 18 pages
https://doi.org/10.1155/2018/2862143

Research Article

Investigation on Derailment of Empty Wagons of Long Freight Train during Dynamic Braking

Xin Ge, Kaiyun Wang, Lirong Guo, Min Yang, Kaikai Lv, and Wanming Zhai

State Key Laboratory of Traction Power, Southwest Jiaotong University, Chengdu 610031, China

Correspondence should be addressed to Kaiyun Wang; kywang@swjtu.edu.cn

Received 15 June 2018; Accepted 2 August 2018; Published 6 September 2018

Academic Editor: Matteo Strozzi

The derailments of empty wagons of long freight trains frequently occurred around the world, which caused tremendous losses every year. Aiming at an actual derailment of empty wagons on straight line during dynamic braking, the field investigation was conducted to find the reasons of the accident. According to the investigation results, the large coupler yaw angle and coupler force, the special connection mode by drawbars, as well as the poor conditions of wheel treads and flanges were supposed to be responsible for the accident. The simulaiton model composed of 3 C_{80}-type gondolas, and two RFC-type drawbars is established, the accuracy of which is validated by the field experimental test. When the wheel-rail friction coefficient is set to be 0.7 and the coupler forces are set to be 350 kN with a coupler yaw angle of 7 degrees, the simulation results are consistent with the field investigation results. Simulation results indicate that the coupler yaw angle, coupler force, and wheel-rail friction coefficient have significant influences on the derailment. The increasing coupler yaw angle and coupler force will increase the risk of derailment. For the wagon units adopting the drawbars, the riskiest wagon changes from the middle wagon to the front one as the lateral components of the coupler forces increase. A large wheel-rail friction coefficient can raise the risk of derailment. However, an overlarge friction coefficient will decrease the derailment risk. According to the field investigation and simulation results, the wheel-rail friction coefficients should be limited below 0.5 to ensure the running safety of empty wagons. Besides, the operations of the train should be optimized to avoid large coupler yaw angle and coupler force.

1. Introduction

Railways is recognised worldwide as one of the safest transportation. However, derailment accidents occur occasionally, which cause tremendous casualties and property loss around the world every year. Statistics from Australia revealed that the freight trains account for vast majority of mainline derailments [1]. Moreover, the empty condition is much riskier than the loaded condition on the consideration of the derailment issue for the freight train, especially in the braking mode [2]. Researchers carried out a great deal of studies on that, but the factors that resulted in derailment remained to be investigated currently. It is of great significance to conduct investigation on derailment of empty wagons.

Since Nadal proposed the derailment evaluation criterion (the Nadal limit) in 1896, the scholars all over the world have studied the train derailment and got great achievements. Based on Nadal's research work, Weinstock [3] comprehensively considered the lateral force to vertical force ratio of two wheels on the same axle and put forward a less conservative criterion which was adopted as an evaluation criterion of derailment by ARR (Association of American Railroads). Researchers at JNR (Japanese National Railway) conducted a series of theoretical and experimental research on derailment. The derailment evaluation criterion of JNR distinguishes the climb derailment from jump derailment by the duration of lateral force impulse [4]. Zhai [5] simulated single-wheelset derailment and full-scale freight vehicle derailment based on vehicle-tack coupled dynamics theory. According to the simulation results, Zhai suggested a modified derailment evaluation criterion based on the derailment coefficient and rate of wheel load reduction by introducing the duration that the indexes exceed the limits. Besides, a method for evaluating the wheel derailment based on the variation of wheel vertical rise was proposed [6]. Apart from the derailment evaluation criterion, derailment mechanism and preventive measures are also research hotspots. Zeng

et al. [2, 7] put forward a new set of theory for train derailment analysis based on the theory of random energy analysis and made significant achievements. Nagase et al. [8] conducted a model experiment according to the wheel climb derailment on the steep curve at low speeds. The influence of adhesion coefficient on the wheel climb derailment was analysed. Zeng et al. [9, 10] studied the wheel flange climb derailment based on theoretical analysis and a single-wheelset test stand. It was revealed that large wheel lateral force and reduced vertical force were responsible for the wheel climb derailment. By means of simulations and experiments, Wang et al. [11–15] optimized the coupler structures and suspension parameters to enhance the running safety and stability of long freight trains. Cole and Wu et al. [16–18] focused on the longitudinal dynamics performance of the long freight train and had done excellent work on longitudinal dynamics simulation. Durali and Shadmehri [19] established a nonlinear comprehensive model to predict derailment in different operating conditions. Hung et al. [20] developed a technique for detecting the early signs of the derailment of a railway vehicle. Besides, postderailment devices were designed to limit the extent of derailment, and relevant experiments were carried out to validate its effectiveness [21, 22].

The previous research mainly concentrated on the derailment of a single-wheelset or vehicle; however, the influence of coupling devices on running performance of vehicle cannot be neglected. Based on an actual derailment accident, this paper focuses on the empty wagons of a long freight train and studies the influence factors of derailment during dynamic braking. Firstly, the field investigation results of the accident are presented, and the theoretical analysis for potential causes of derailment is conducted. Then, the derailment simulation model considering the coupling devices has been established, and the field test results are adopted to validate the accuracy of the simulation model. Finally, the influence laws of the coupler yaw angle, coupler force, and wheel-rail friction coefficient on the derailment are analysed based on the simulation model.

2. Field Investigation on the Derailment

2.1. Background. A derailment accident occurred on a train consisting of 2 double-unit SS4-type locomotives and 105 C_{80}-type gondolas during dynamic braking. The wagons were empty when the accident occurred. The accident region is located at a downhill section with the gradient ranging from −0.28% to −0.14%. The dynamic braking was applied with 60% braking forces at the initial braking velocity of 73 km/h while the train just entered a sharp curve with a radius of 400 meters. Under the continuous braking forces, the train passed through the curve and a turnout area successively before reaching the accident site. The accident wagons derailed on a straight track while the velocity of the train was reduced to 36 km/h. As a result, the fifth wagon behind the locomotives climbed onto the top of the railhead and derailed subsequently and then pulled the adjacent wagons out of the track.

Figure 1(a) shows the main condition of accident site. It is seen that the train suffered tremendous destruction, and the bogies were separated from the car bodies. Figure 1(b) shows the coupler of the accident wagon, and obvious crack on coupler yoke is observed. The yellow zones in Figure 1(c) show clear moving traces of the wheel on rail surface. It is seen that the wheel climbed onto the rail along the inside surface gradually and moved forward on the top of the railhead for a short distance and then derailed.

2.2. Structural Characteristics of the Train. It is aforementioned that the train consisted of 2 double-unit SS4-type locomotives and 105 C_{80}-type gondolas, where every three C_{80}-type gondolas composed a 3-pack connected by RFC-type drawbars. The 3-packs were connected by interlock couplers, which were composed of No. 16 rotary coupler and No. 17 nonrotary coupler.

2.2.1. C_{80}-Type Gondola. The C_{80}-type gondolas are widely applied in Chinese heavy haul railways, mainly for the transport of coals. The car body of the wagon is the double-bathtub structure and has the characteristics of low dead load, large volume, as well as high load-carrying capacity. The load-carrying capacity reaches approximately 80 tons. The gondola is equipped with two K6-type bogies. The bogie is a typical three-piece bogie, which is mainly made up of two wheelsets, two side frames, one bolster, suspension system, and attachments. The suspension system of the bogie is primarily composed of coil spring groups with two-stage stiffness and wedge friction damper. Besides, the rubber blankets are mounted on the adapters to provide adequate locating stiffness, and the cross-sustaining device is equipped to enhance the diamond-resistant rigidity and hunting stability. The detailed structures of the K6-type bogie are shown in Figure 2.

2.2.2. The Coupling Devices. The interlock couplers, composed of the No. 16 rotary coupler and the No. 17 nonrotary coupler, are specially designed for the 10,000-ton train. The cooperation of these two couplers enable the wagons to rotate 180 degrees around the longitudinal centre line of the couplers without decoupling, which can dramatically improve the unloading efficiency. Figures 3(a) and 3(b) show the structures of the No. 16 rotary coupler and the No. 17 nonrotary coupler, respectively. The two couplers have the same coupler head, but the coupler shanks of the two couplers are different. The coupler tail of the No. 17 nonrotary coupler is a spherical structure with an adjusting shoulder. The shoulder provides the coupler with self-centring ability. Unlike the No. 17 coupler, the adjusting shoulder of the No. 16 coupler is abolished to ensure the flexible rotation of the coupler. Besides, the shank of No. 16 coupler is designed to be cylindrical to reduce rotational resistance.

For a long freight train, it is difficult to eliminate the longitudinal impulse arose from the traction and braking operations because of the existence of the coupler slacks. The drawbars replace the couplers with a bar-shape casting to eliminate the coupler slack, which can dramatically improve the longitudinal dynamics performance of the train. To balance the curve negotiation and longitudinal dynamics performance of the train, only a part of couplers is substituted

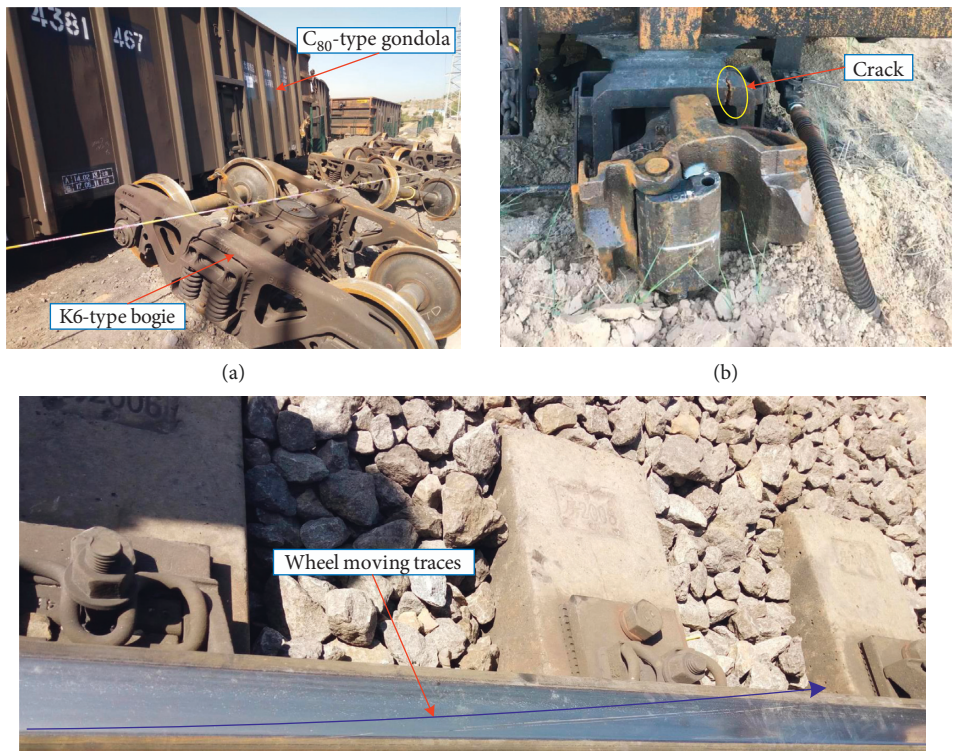

Figure 1: The field investigation: (a) the scene of derailment accident; (b) crack on coupler yoke; (c) wheel moving traces.

with drawbars. The RFC-type drawbars are specially designed to exchange the interlock couplers. The end structures of the drawbars are designed the same as the corresponding structures of No. 16 and No. 17 couplers; thus the drawbars can exchange the interlock couplers without any auxiliary devices; the structure of the drawbar is shown in Figure 3(c).

The couplers (or drawbars) can only implement the connection of the adjacent wagons (or locomotives). To get better coupling performance, the draft gear is indispensable. The MT-2 draft gear, a typical spring friction draft gear, is adopted. The main parameters of the MT-2 draft gear are listed in Table 1.

2.3. Analysis of the Accident Causes. It is seen in Figure 1(a) that the structures of the main components of the bogies are basically undamaged without obvious cracks. Therefore, the possibility that the structural failure caused the derailment could be eliminated preliminarily. As aforementioned that the derailment happened during dynamic braking, it is known that the dynamic braking forces were only applied to the locomotives, which led to inevitable longitudinal impulse, especially for the long freight train. Moreover, the dynamic braking was applied as the train just entered a sharp curve, which might cause large coupler yaw angles affected by the coupler forces and track irregularities. Under the effect of the continuous braking forces, the couplers could not get back to centring position even when the train left the curved track. As the train moved forward into the turnout area, the lateral wheel/rail impact in switch rails and frogs would have caused the yaw motion of the car bodies, which might increase the

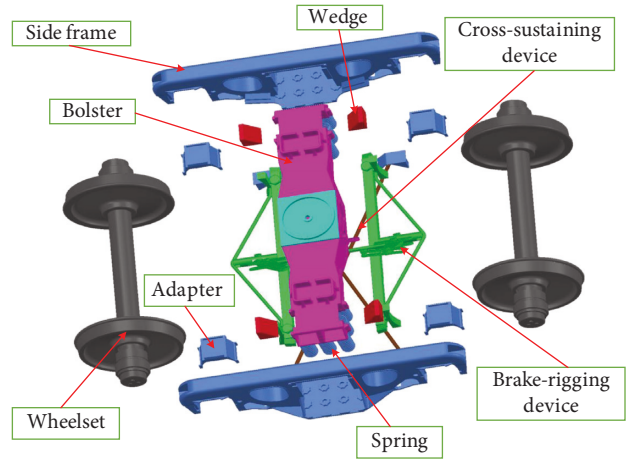

Figure 2: Structure diagram of K6-type bogie.

coupler yaw angles. Besides, the back-up braking system came into operation when the train velocity was reduced to 36 km/h. The braking current fluctuated a lot, which resulted in the fluctuation of braking forces. The longitudinal impulse of the train was intensified, which affected the safety and stability of the vehicles remarkably. It is seen in Figure 1(b) that there exists an obvious crack on the coupler yoke, which demonstrates that the coupler yaw angle reached its maximum, and large lateral force was applied on the coupler yoke during derailment. It can be speculated that the large coupler yaw angles and coupler

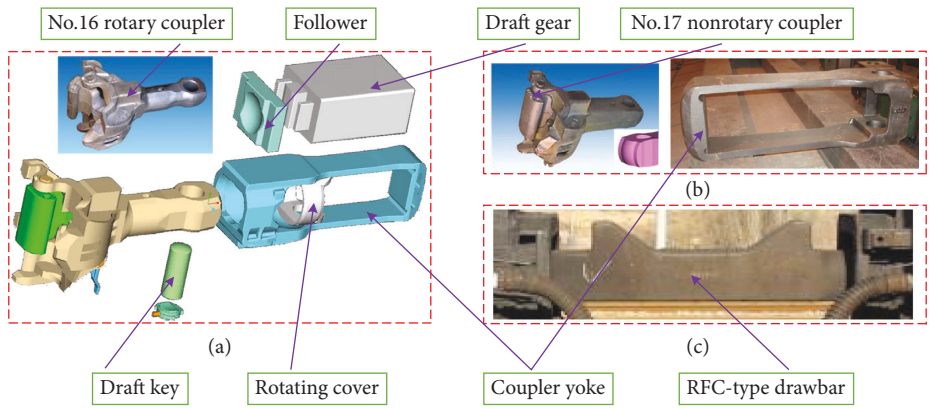

Figure 3: The structure diagram of coupling devices and draft gear system: (a) no. 16 rotary coupler; (b) no. 17 non-rotary coupler; (c) RFC-type drawbar.

forces may be one of the most critical influence factors for the accident.

As introduced, the internal connection of the 3-pack is accomplished using the drawbars. Comparing with the couplers, the drawbars have stronger constraints on the lateral and vertical degree of freedoms (DOFs) of the middle wagon. Moreover, the wagons were empty when the derailment happened. Under the effect of large longitudinal impulse, the nontread contact and wheel lift are more likely to happen to the middle wagon of the 3-pack. This is regarded as the second potential influence factor for the accident.

Investigations on accident wagons revealed that the poor conditions of wheel treads and flanges might be the third important influence factor of the accident. Figure 4(a) shows abrasion marks on the wheel flange and tread surface. The red zones appear to have material loss, which may result from postderailment dynamics behaviour. The yellow zones show obvious contact traces, which demonstrate the intense interaction between the wheel flange and rail. Besides, the wheel tread and flange surface of the accident wagons were rougher in comparison with that of the normal wagon, as shown in Figure 4(b). The further investigation shows that the wheel truing was just completed not long before the accident. Relevant research studies indicate that the cutting traces caused by wheel truing can increase the wheel surface roughness, which may raise the risk of flange climb derailment [23]. The surface condition of wheel tread and flange affect the contact status between the wheel and rail remarkably. The rougher wheel tread and flange will result in a higher coefficient of friction at wheel-rail, which enables the rail to provide adequate climbing force for the wheel. According to the Nadal single-wheel L/V limit criterion [24], the critical value of the derailment coefficient (L/V) in static equilibrium state can be calculated by

$$\frac{L}{V} = \frac{\tan\delta - \mu}{1 + \mu\tan\delta}, \quad (1)$$

where L is the lateral force applied to the wheel, V is the vertical force applied to the wheel, μ is the wheel-rail friction coefficient, and δ is the wheel flange angle. It is obvious that the critical value of the derailment coefficient will decrease as the friction coefficient μ increases, which means that the wheel is riskier to climb onto the top of the railhead.

Table 1: The main parameters of MT-2 draft gear.

Items	Value	Unit
Maximum impedance force	2000~2300	kN
Draft gear stroke	83	mm
Draft gear capacity	54~65	kJ
Absorbed energy	46~55	kJ
Absorption ratio	≥80	%
Mass	175	kg

According to the abovementioned analysis, it was concluded that when the train was running on a sharp curve, the synthetic action of the dynamic braking operation and track irregularities caused large coupler yaw angles; furthermore, the lateral wheel/rail impulse in the turnout area led to the further increase of the coupler yaw angles. When the longitudinal force was transmitted to the coupler, a large lateral component force was generated. The lateral component force caused a large wheelset lateral force, which made the wheel flange approach the rail and contact it subsequently. Under the comprehensive effects of the continuous large components of the lateral coupler forces, the poor conditions of wheel treads and flanges, and the limitation of the drawbars on lateral and vertical DOFs of the middle wagon, the middle wagon of the 3-pack climbed onto the rail gradually and moved forward on the top of the railhead for a short distance, and then derailed.

3. Simulation Model

In order to validate the above analysis and to study on the influence of the potential factors on derailment of empty wagons, a derailment simulation model considering the coupling devices was established based on multibody dynamics theory. The model was composed of the longitudinal dynamics model and 3-pack model. Since the coupler forces cannot be obtained when the accident happened, the longitudinal dynamics model of the train was employed to calculate the coupler forces firstly, and then the coupler forces were applied on car bodies of the 3-pack model.

(a) (b)

Figure 4: Wheel surface condition: (a) the abrasions on wheels of the accident wagon; (b) the comparison of the accidental and normal wheels.

3.1. Longitudinal Dynamics Model

3.1.1. Longitudinal Train Model. According to prior research studies [16–18], the train model is established, as shown in Figure 5. Each wagon (or locomotive) is considered as a detached body with only the longitudinal DOF. The total DOFs of the longitudinal dynamics model are equal to the sum of the locomotives and wagons. Both interlock couplers and drawbars are modelled as a nonlinear stiffness and damper with a gap element for the coupler slack. It should be noted that the gap should be set as zero for the drawbars.

In Figure 5, m = vehicle mass, kg; F_C = coupler force, N; F_W = sum of retardation forces, N; F_{TE} = traction force from a locomotive unit, N; F_{DB} = dynamic brake force from a locomotive unit, N; F_B = air brake force, N; X = vehicle displacement, m; and α = track grade. The sum of retardation forces, F_W, is composed of rolling resistance, curving resistance, air resistance, and gravity force components due to the track grade and starting resistance.

According to the train model, the longitudinal dynamic differential equations are developed as [18]:

For the lead vehicle

$$m_1\ddot{X}_1 = F_{C1} - F_{W1} + F_{TE1} - F_{DB1} - F_{B1}. \quad (2)$$

For the ith vehicle

$$m_i\ddot{X}_i = F_{Ci-1} - F_{Ci} - F_{Wi} + F_{TEi} - F_{DBi} - F_{Bi}. \quad (3)$$

For the nth or last vehicle

$$m_n\ddot{X}_n = F_{Cn-1} - F_{Wn} + F_{TEn} - F_{DBn} - F_{Bn}, \quad (4)$$

where i is the number of the wagon (or locomotive).

3.1.2. Vehicle Connection Model. As the most important components in longitudinal dynamics model, the modelling of connection elements between wagons (or locomotives) determines the accuracy of simulation results. Research studies conducted by Cole and Wu et al. indicate that the impendence forces appear to have evident differences between the loading and unloading process (called hysteresis characteristics) [16–18]. In the vehicle connection model, the nonlinear hysteresis characteristics of the draft gear are intensively considered. The current models of the friction-type draft gear consider the detailed frictional characteristic according to the real structures. The model is usually complicated with several parameters, and the accuracy of simulated results is remarkably affected by the values of the parameters. Generally, the values of the parameters need to be modified according to a serial of experiments. In this paper, a universal simplified velocity-dependent model of draft gear is employed, as shown in Figure 6(a), and the accuracy of the model in longitudinal dynamics simulation has been validated by Liu et al. [25]. The impedance forces of loading and unloading processes are defined as $f_l(\Delta x)$ and $f_u(\Delta x)$, respectively, where Δx is the draft gear stroke ($\Delta x = 0$ for drawbars). The discontinuity point appears when the draft gear switches between loading and unloading processes; therefore, a velocity-dependent impedance force, $F_c(\Delta x, \Delta v)$, is defined as follows [26]:

$$F_c(\Delta x, \Delta v) = \begin{cases} f_l(\Delta x), & (\Delta v \geq ev), \\ f_m(\Delta x) + [f_l(\Delta x) - f_m(\Delta x)]\dfrac{\Delta v}{ev}\operatorname{sign}(\Delta v), & (-ev < \Delta v < ev), \\ f_u(\Delta x), & (\Delta v < -ev), \end{cases} \quad (5)$$

$$f_m(\Delta x) = \frac{f_l(\Delta x) + f_u(\Delta x)}{2},$$

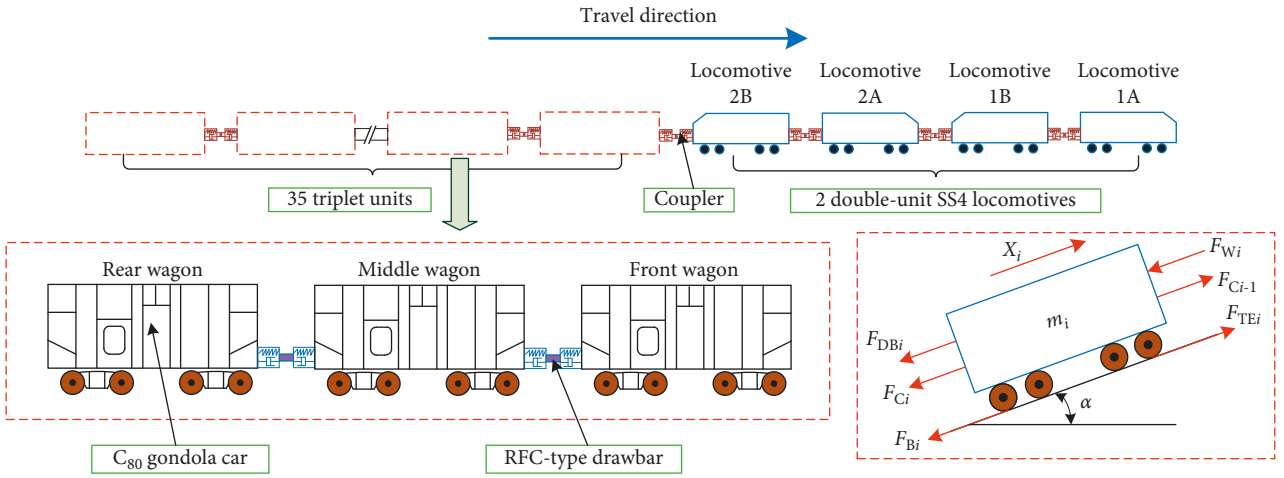

Figure 5: The longitudinal train model.

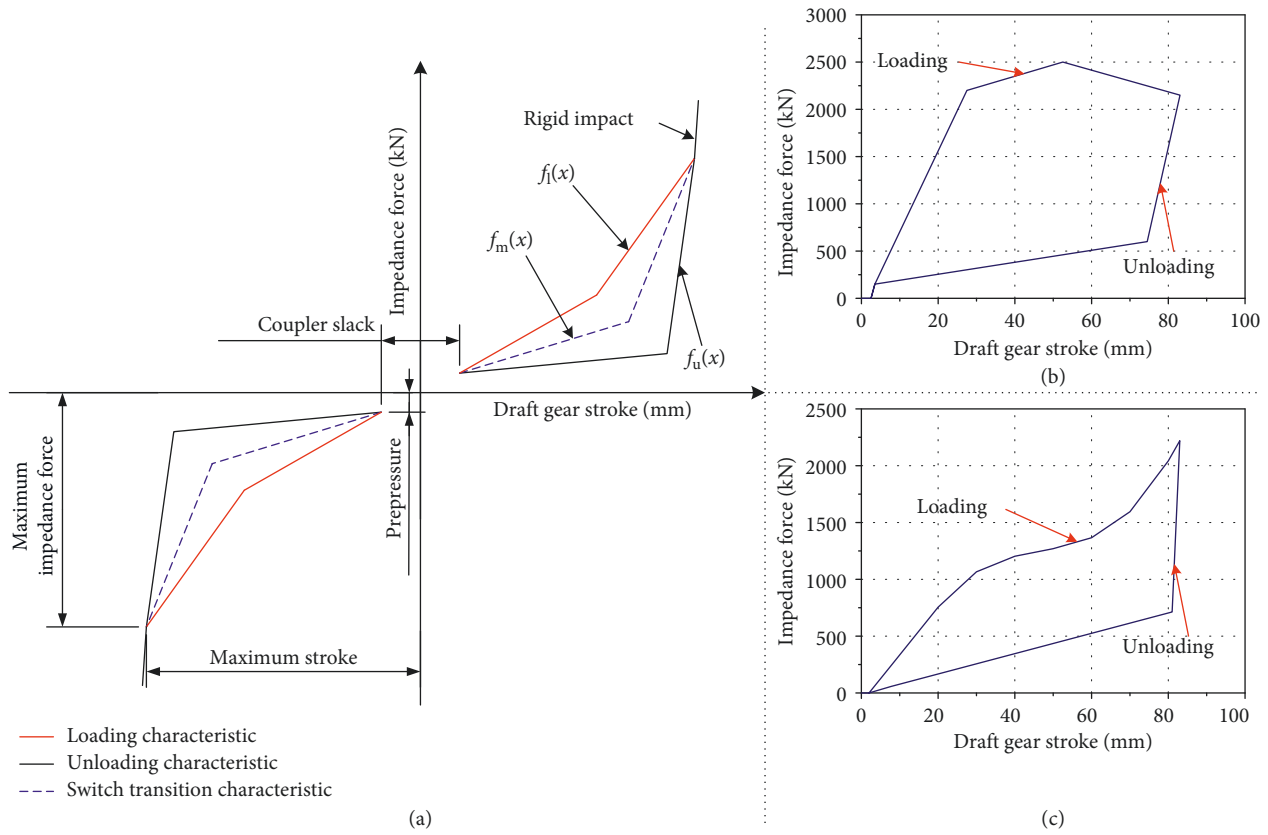

Figure 6: Draft gear: (a) the velocity-dependent model; (b) the nonlinear hysteretic characteristics of the QKX100 graft gear; (c) the nonlinear hysteretic characteristics of the MT-2 graft gear.

where Δv is the change rate of draft gear stroke, and ev is the switch velocity which determines the switch between loading and unloading processes. It should be noted that the direction of the resistance force of the draft gear is always opposite to that of the relative motion; hence, the function sign (Δv) is introduced to describe the characteristics.

The nonlinear hysteresis characteristics of the QKX100 draft gear for the locomotive and the MT-2 draft gear for wagons are shown in Figures 6(b) and 6(c), respectively. The loading and unloading characteristics, $f_l(\Delta x)$ and $f_u(\Delta x)$, as well as the switch velocity ev are acquired by measurements [8]. The margins between the loading and unloading curves illustrate the nonlinear hysteresis characteristics which capacitate the graft gear to absorb vibration energy [14].

3.2. Dynamic Model of the 3-Pack. The 3-pack model consists of 3 C_{80}-type gondolas and 2 RFC-type drawbars as well as

assorted draft gears, which is established using the multibody dynamics software SIMPACK, as shown in Figure 7.

3.2.1. Single C_{80}-Type Gondola Dynamic Simulation Model. The single C_{80}-type gondola model has 62 DOFs, and each of the car body, the side frame, and the wheelset has six DOFs, while the adapters are connected to the axles with only one rotational DOF around the Y-axis, and the bolster is allowed to move vertically and to yaw relative to the car body. The friction between the side bearings and centre plates are simulated using the No. 100 nonlinear friction force element of the SIMPACK. The friction force is calculated based on Coulomb's friction law.

$$F_T = \begin{cases} -\mu_0 F_N, & v_r \le -v_f, \\ \dfrac{|v_r|}{v_f}\mu_0 F_N \operatorname{sign}(v_r), & -v_f < v_r < v_f, \\ \mu_0 F_N, & v_r > v_f, \end{cases} \tag{6}$$

where F_T is the friction force, μ_0 is the friction coefficient between the contact surfaces, F_N is the normal contact force, v_r is the relative velocity of contact region, and v_f is the critical velocity of the static friction. The wedge suspensions are one of the most important components in the wagon. Figure 8(a) shows the wedge suspension structures of the K6-type bogie. In this paper, the wedge suspension is detailed modelled according to its structures, as shown in Figure 8(b). It is composed of wedges, column wear plates, bolster, central springs, and damping springs. The column wear plates are fixed together with the side frame. The bolster and wedges are connected with the side frame by the central springs and damping springs, respectively. The friction between the bolster the wedges is modelled using the No. 100 nonlinear friction force element, so does the friction between the wedges and column wear plates. The coil spring groups with two-stage stiffness are modelled as spring elements with variable stiffness using the No. 5 force element. Figure 8(c) shows the details of the wedges and the coil spring groups. Each side of the wedge suspension contains nine spring sets. The seven spring sets in the red zone are named central springs, and the other two spring sets are called damping spring. For the front and rear wagons, the coupler forces are applied on the places where the couplers are installed using the No. −98 marker, which follows the track at the position of a track joint with the defined offsets. The main parameters of empty C_{80}-type gondola model are listed in Table 2.

3.2.2. Model of the RFC-Type Drawbar and Draft Gear System. The model of the RFC-type drawbar and draft gear system consists of the drawbar with spherical contact surfaces, the followers, MT-2 draft gears, and the coupler yokes. The drawbar has the freedom to move longitudinally, to yaw, and to pitch. The follower has only 1 DOF in the longitudinal direction. The MT-2 draft gear is modelled as a force element with hysteresis characteristics as in Figure 7 using the No. 104 nonlinear element. It is noted that the coupler slack

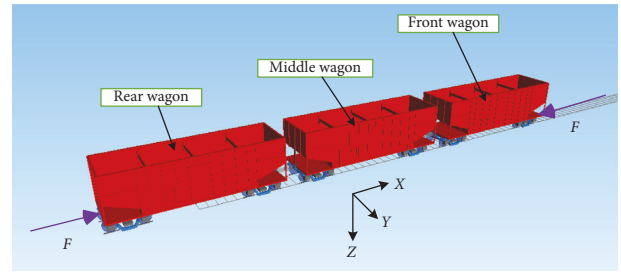

Figure 7: Dynamic model of the 3-pack.

should be set as zero. The coupler yoke is modelled as a restoring moment with stop characteristics using the No. 13 force element. The restoring moment, T_r, is described as

$$T_r = \begin{cases} 0, & |\gamma| < \gamma_{free}, \\ l[\gamma - \gamma_{free} \cdot \operatorname{sign}(\gamma)] \cdot K_{tr}, & |\gamma| \ge \gamma_{free}, \end{cases} \tag{7}$$

where γ is the rotation angle of the drawbar, γ_{free} is the maximum free rotation angle, l is the longitudinal distance between the two pin holes of the drawbar, and K_{tr} is the angular stiffness of the modelled torsional spring, 10^8 N/rad. Both yaw and pitch stoppers are set at drawbar tails, where the maximum free angles of yaw and pitch are 13° and 6°, respectively. Besides, the No. 18 contact force element and the No. 100 nonlinear friction element are employed to simulate the contact between the follower and drawbar tail.

3.2.3. Validation of the 3-Pack Model. It is significant to validate the simulation model before further analysis. Hence, the field test results are adopted to compare with the simulation results.

The experimental test was performed on a straight ballast track in the Dazhun Railway. The test section adopts Chinese 60 kg/m rails, and the gauge is 1435 mm. The test train is composed of 2 double-unit SS4-type locomotives and 105 empty C_{80}-type gondolas. The middle wagon of the first 3-pack behind the locomotives has been chosen as the test wagon. The displacement sensors are installed on the side frame of the test wagon to detect the dynamic displacements of the car body and the bogie. The acceleration sensor is installed on the centre sill of the car body underframe to measure the acceleration of the car body. The employed sensors in this test are illustrated in Figure 9.

During the test, the dynamic braking was applied at the initial velocity of 78 km/h, while the whole train was located on a straight track. The braking force increased gradually from 0% to 70%. The simulation conditions are set to be consistent with the tested one. The initial velocity of the train is set to be 78 km/h, and the wheel-rail friction coefficient is set to be 0.3. The American 5-level track irregularities are adopted. The coupler forces are determined by simulation as shown in Figure 10, and the coupler yaw angle is set to be zero. Figure 11 shows the comparatives of the simulation and the test results. It is seen in Figures 11(a) and 11(b) that the simulated and the tested acceleration of the car body are basically consistent in time domain, and acceleration

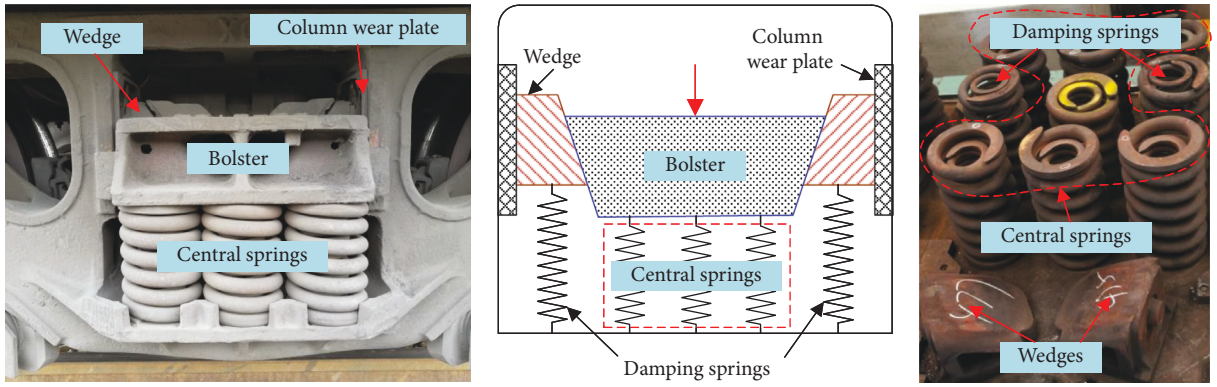

(a) (b) (c)

Figure 8: Wedge suspension of the K6-type bogie: (a) structure diagram; (b) dynamic model; (c) details of the wedges and the coil spring groups.

Table 2: The main parameters of empty C_{80}-type gondola.

Item		Value	Unit
Wagon mass		10297	kg
Axle load		25	t
Wheel base		1.83	m
Bogie distance		8.2	m
Length over pulling faces of couplers		12	m
Coupler height		0.88	m
Wheel radius		0.42	m
Primary suspension stiffness (signal adapter)	Longitudinal	13	MN/m
	Lateral	11	MN/m
	Vertical	160	MN/m
Secondary suspension stiffness (one side in a bogie)	Longitudinal	1.818	MN/m
	Lateral	1.818	MN/m
	Vertical	2.233	MN/m
Axial stiffness of the cross-sustaining device		14.8	MN/m
Prepressure of side bearings		19.8	kN

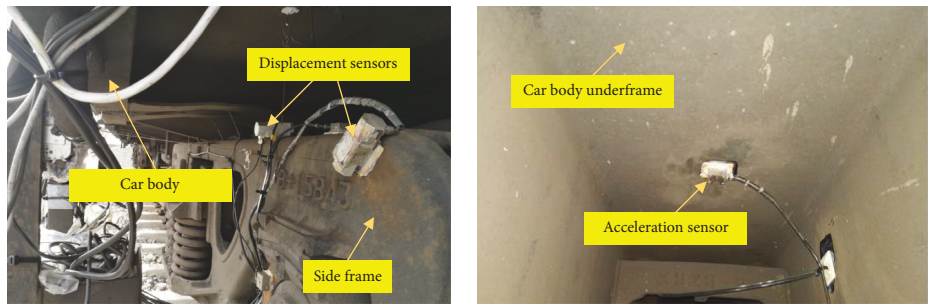

(a) (b)

Figure 9: Instruments of the sensors: (a) displacement sensors on the side frame; (b) acceleration sensor on the car body.

amplitudes do not differ a lot. The vertical accelerations are predominantly within 0~0.3 g, while the lateral accelerations are within 0~0.1 g. Figures 11(c) and 11(d) show the comparisons of the lateral and vertical relative displacement between the side frame and the car body, respectively. Both the tested and simulated lateral displacements are mainly distributed in −2~2 mm, and the distribution range of the vertical displacement is close to it. However, the maximums of the vertical displacement approach 4 mm, which is around twice of the maximal lateral displacements.

It should be noted that the true track irregularities have randomness, and the differences between the adopted American 5-level track irregularities and the true conditions cannot be avoided. According to the above analysis, it can be concluded that the simulation model can simulate the dynamic behaviour of the 3-pack during dynamic braking.

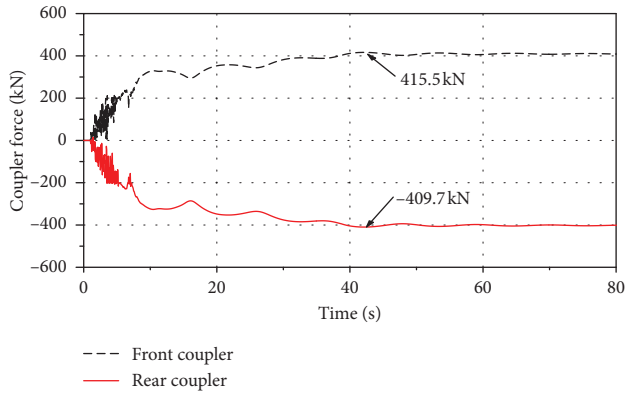

Figure 10: The simulated coupler forces for validation.

4. Results of Derailment Simulation

4.1. Longitudinal Dynamic Simulation. According to the field investigation results, the dynamic braking operation is applied with 60% braking force at the initial velocity of 73 km/h. Figure 12 shows the velocity and the coupler forces of the second 3-pack during the dynamic braking. The train velocity does not change immediately, and the coupler forces fluctuate a lot at the initial 13 seconds. Then the train velocity decreases linearly, while the coupler forces increase rapidly over time. It is seen that the train velocity reaches 36 km/h at around the 68th second, while the front and rear coupler forces are about 350.1 kN and −346 kN, respectively.

4.2. Derailment Simulation and Analysis

4.2.1. Calculation Conditions. The process of derailment is very short; hence, the velocity and coupler forces of the 3-pack are assumed to be constant. According to the field investigation results, the velocity is set as 36 km/h. Based on the longitudinal dynamics simulation, the coupler forces are determined as 350 kN when the velocity decreases to 36 km/h. The straight track with the American 5-level track irregularities is used. As previously analysed that the coupler yaw angle might be an important influence factor, however, the real coupler yaw angle during the derailment cannot be obtained. The field test was conducted to measure the coupler yaw angle of the 3-pack, and the displacement sensors were installed on the car body to detect the variation of the angle as shown in Figure 13(a). The accident section was chosen as the test section, and the train passed through it in the traction mode at around 70 km/h. It can be seen in Figure 13(b) that when the train passed through the sharp curve and the turnout area successively, the maximal coupler yaw angle in the curve and turnout area reached 4.35 degrees and 5.72 degrees, respectively. Moreover, the yaw angle of the drawbar in the braking mode is supposed to be larger than that in the traction mode in general. Comprehensively considering the above factors and the fact that the wagons derailed, the coupler yaw angle is assumed to be 7 degrees. In the model of the 3-pack, two equal coupler forces are applied on both ends of the 3-pack in the opposite direction with a constant yaw angle of 7 degree. The coupler forces are set to increase linearly from 0 to 350 kN ($t = 5$~10 s) and keep constant ($t = 10$~15 s).

Besides, the abnormal roughness of the wheel tread and flange is taken into account by increasing the wheel-rail friction coefficient of the 3-pack. It can be seen from Figure 4(b) that there exist obvious cutting traces on the wheel tread and flange of the accident wheel, and the surface of the normal wheels is very smooth. Thus, the wheel-rail friction coefficient of the accident wagon is larger than that of the normal. According to Japanese research studies, the normal wheel-rail friction coefficient ranges from 0.3 to 0.5 under the conditions of low velocity and dry environment [27]. Since the real wheel-rail friction coefficient is difficult to be measured, the friction coefficient is assumed to be 0.7 in the calculation. For the wheel profile, the measured profile cannot represent the real condition of wheel profile because of the intense wear during the derailment process. As aforementioned that the wheel truing was completed not long before the accident, the standard LM-type wheel tread is adopted.

4.2.2. Derailment Evaluation Criterion. Research studies indicate that the derailment can only occur under the circumstance of continuous severe wheel-rail interaction [28, 29], and the commonest Nadal single-wheel L/V limit criterion is proved to be conservative for evaluating derailment [23]. A new method for evaluating derailment based on the variation of wheel vertical rise was adopted in this paper [6]. The wheel vertical rise is defined as the vertical distance between the nominal contact point of the wheel tread and the highest point on the top of the railhead. The wheel vertical rise Z_{up} is composed of the climb height Z_1 and the jump height Z_2 (only when the wheel is separated from the wheel) as shown in Figure 14. The derailment evaluation criterion based on the wheel vertical rise is defined as

$$Z_{up} < h_f, \tag{8}$$

where h_f is the wheel flange height. The flange height of the Chinese LM-type tread is 27 mm. It is noted that derailment of a wheelset is generally accompanied with a large lateral wheelset displacement. If the wheel vertical rise exceeds the wheel flange height under the condition of small lateral displacement, the wheel will fall back to the rail affected by gravity and the derailment will not happen [2]. Hence, the wheel vertical rise and lateral wheelset displacement must be taken into account simultaneously for evaluation of derailment. According to Durali's research [30], the critical value for allowable lateral wheelset displacement of the Chinese LM-type tread is 54 mm. When the lateral wheelset displacement exceeds the limitation, the lateral constraint of rails disappears, and the trend of derailment is irreversible.

4.2.3. Analysis of the Derailment Simulation. Figure 15 exhibits the wheel vertical rises and the lateral wheelset displacements of the 3-pack. The dash dot lines in the figure represent the wheel flange contact limitation (half of the play

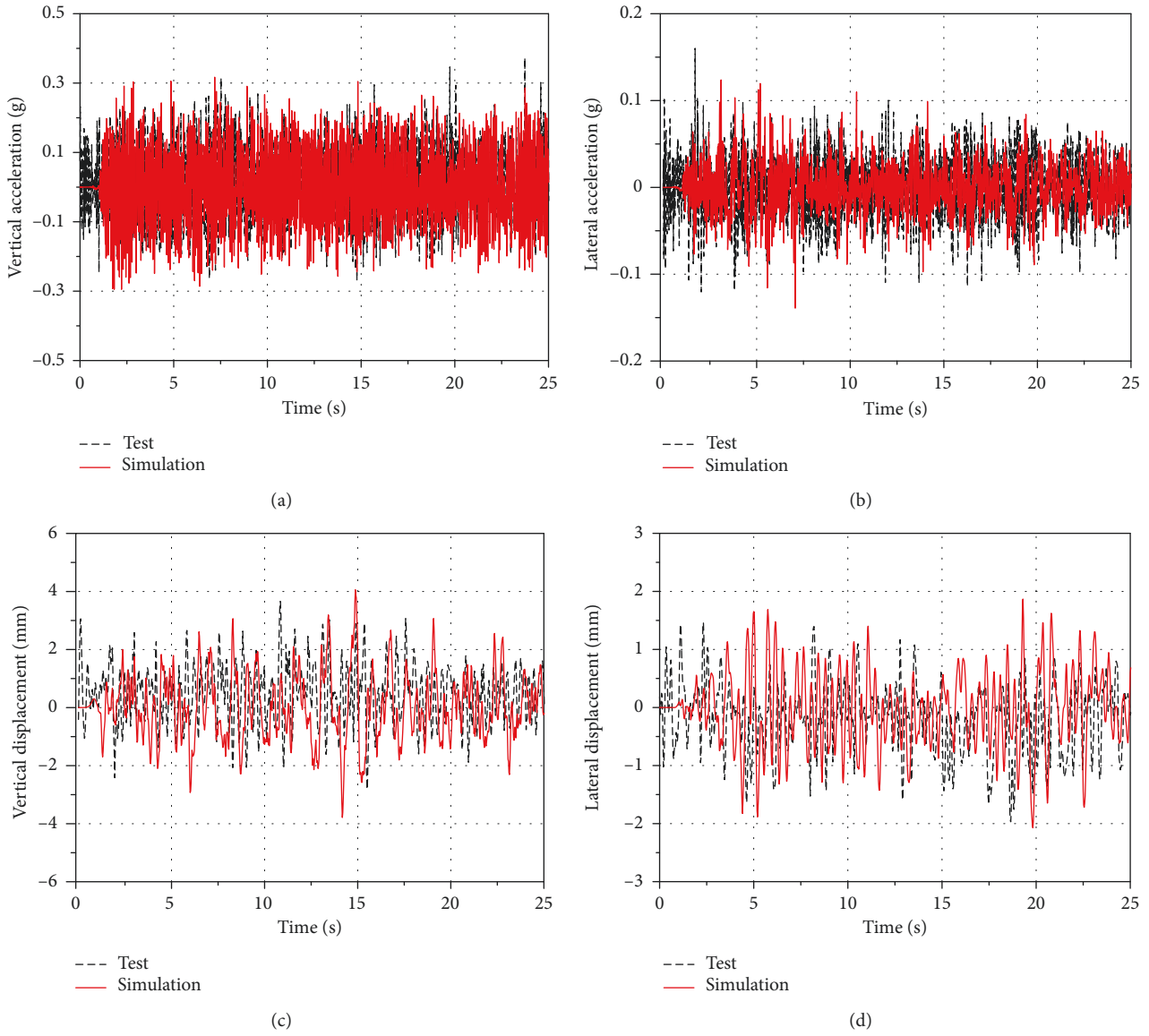

Figure 11: Comparison of the simulated and the tested results: (a) vertical acceleration of the car body; (b) lateral acceleration of the car body; (c) relative vertical displacement between the side frame and car body; (d) relative lateral displacement between the side frame and car body.

between wheel flange and rail). As the lateral wheelset displacement exceeds the limitation, the wheel flange will contact the rail. Figure 15(a) shows the variations of the lateral wheelset displacement, the wheel vertical rise, as well as wheel-rail contact geometry relationships of the middle wagon. It is seen that the simulation period can be roughly divided into three phases:

Phase 1: $t = 0\sim10$ s. The coupler forces increase linearly from 0 to 350 kN during $t = 5\sim10$ s. Affected by the increasing lateral component of the coupler forces, the wheel approaches the rail; the wheel vertical rise and lateral wheelset displacement fluctuate a little and increase gradually to about 3 mm and 7.5 mm, respectively. The wheel flange does not contact the rail.

Phase 2: $t = 10\sim13.5$ s. The coupler forces keep constant at 350 kN. Under the integrated effects of coupler forces and track irregularities, the wheel vertical rise and lateral

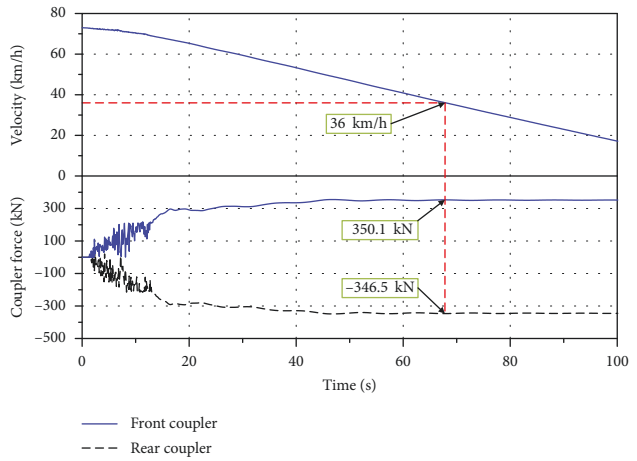

Figure 12: The velocity and coupler forces of the second 3-pack during dynamic braking.

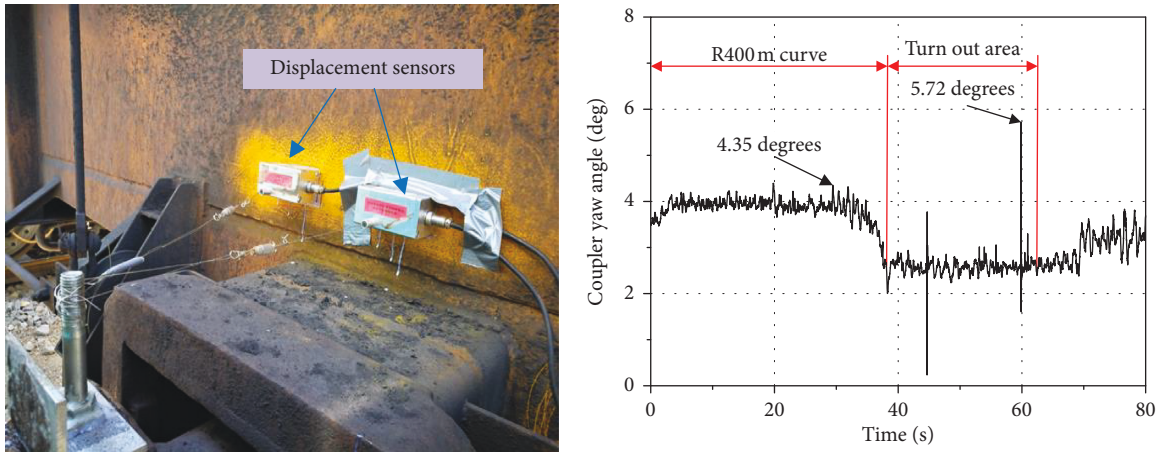

(a) (b)

FIGURE 13: Measurements of coupler yaw angle: (a) displacement sensors for measuring the coupler yaw angle; (b) the measured coupler yaw angle.

wheelset displacement fluctuate a lot. The lateral wheelset displacement exceeds the limitation, and the wheel flange contacts the rail. The maximums of the lateral wheelset displacement and the wheel vertical rise are 16.8 mm and 5.7 mm, respectively.

Phase 3: $t = 13.5$~15 s. The lateral wheelset displacement increases rapidly, while the wheel vertical rise increases sharply to the critical value (about 27 mm) at around $t = 14.8$ s firstly, and then decreases sharply. It can be seen from the figures of wheel-rail contact geometry relationship, the wheel climbs onto the top of the railhead gradually and moves forward for a while, and then gets away from the rail.

It is seen in Figures 15(b) and 15(c) that the lateral wheelset displacements and wheel vertical rises of the front and rear wagons have the similar trend. The lateral wheelset displacements fluctuate in a small range in the initial 8 seconds, and the wheel flanges do not contact the rails. Meanwhile, the wheel vertical rises are very small. Then the lateral wheelset displacements increase rapidly to more than 10 mm, and the wheel flanges contact the rails. During $t = 10$~13.5 s, the lateral wheelset displacements and the wheel vertical rises fluctuate a lot due to the intense wheel-rail interaction, while the lateral displacements keep below 20 mm, and the maximums of the wheel vertical rises are less than 15 mm. As the simulation time exceeds 13.5 seconds, the lateral wheelset displacements and the wheel vertical rises increase sharply. The lateral wheelset displacement of the front wagon reaches its maximum at around $t = 14$ s, and then decreases, while the wheel vertical rise has the same tendency of changes. For the rear wagon, the lateral wheelset displacement and wheel vertical rise increase linearly. The maximal lateral wheelset displacements of the front and rear wagons are less than 28 mm, and the maximums of the wheel vertical rises are about 21 mm. It can be concluded that the front and rear wagons rise along the rails for a distance, but the wheels do not climb onto the top of the railhead.

Figure 16 shows the derailment coefficients, lateral and vertical wheel/rail forces, in the simulation period. It is seen

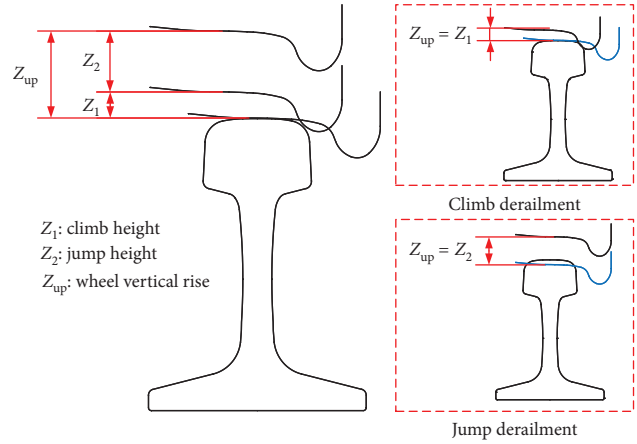

FIGURE 14: The definition of wheel vertical rise.

that the three indexes present the same change law before the middle wagon derails. Under the individual effect of track irregularities, the vertical wheel/rail forces fluctuate more wildly than lateral forces in the initial 5 seconds. Correspondingly, the derailment coefficients vary in a small range. Affected by the increasing coupler forces, all the indexes tend to increase during $t = 5$~10 s, where the index values of the front and rear wagons are generally large than that of the middle wagon. The lateral wheel/rail forces of the front and rear wagons have balanced a part of the lateral components of the coupler force, so the lateral forces applied on the car body of the middle wagon are less than that of the front and rear wagons. As the simulation time exceeds 10 seconds, the index values of different wagons fluctuate within a small range and do not differ a lot. At around $t = 14.8$ s, the derailment coefficient as well as the vertical and lateral wheel/rail forces of the middle wagon decrease sharply to zero, which means the derailment of the middle wagon. It can be seen that the derailment coefficients of all the three wagons have reached the critical value (1.0) in the simulation period; however, only the middle wagon derails, which

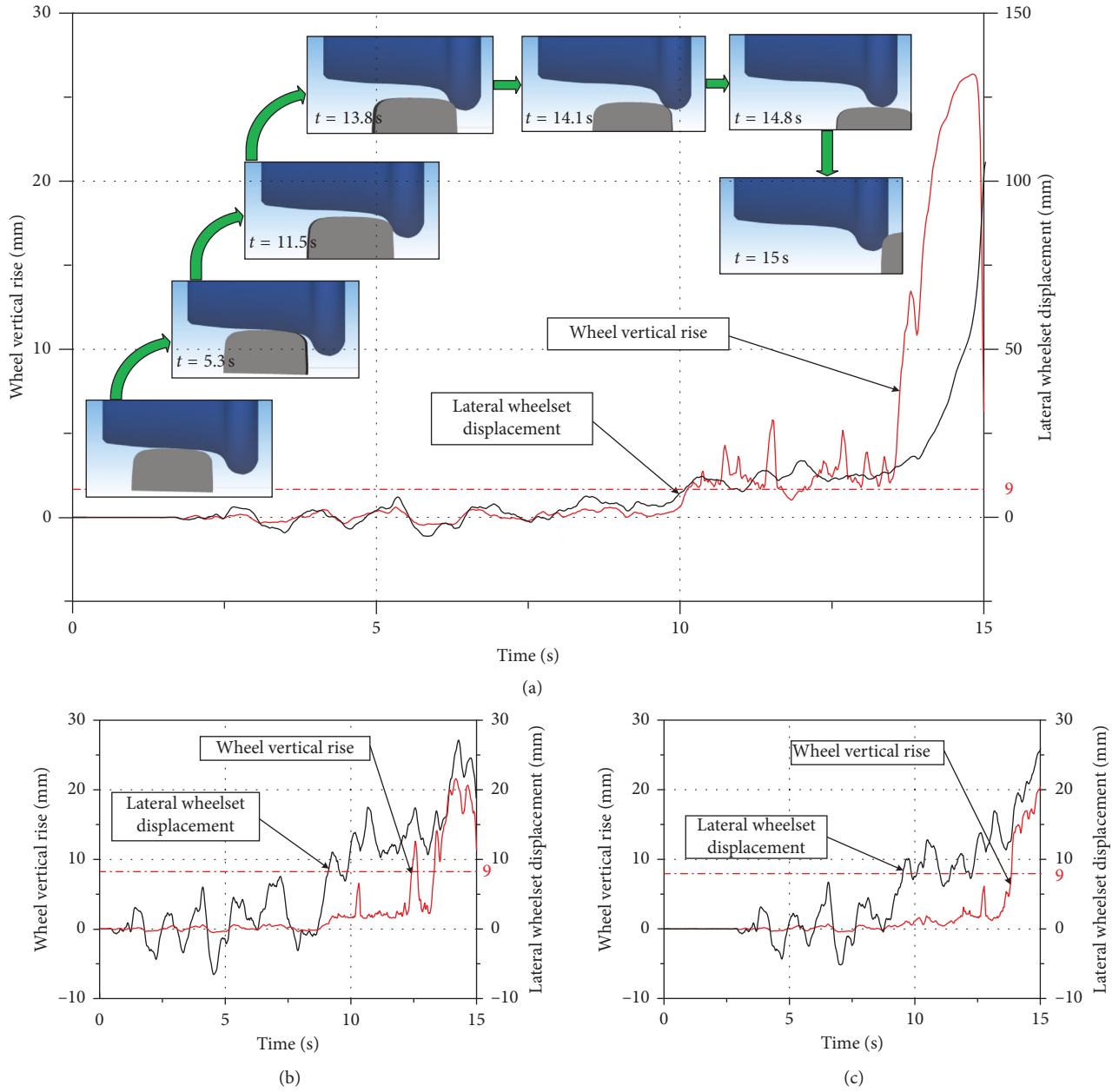

FIGURE 15: Wheel vertical rise and lateral wheelset displacement of different wagons: (a) middle wagon; (b) front wagon; (c) rear wagon.

exactly demonstrates the conservatism of Nadal single-wheel L/V limit criterion.

As mentioned previously, the wagons are connected by drawbars which apply a strong constraint on lateral and vertical DOFs of the middle wagon. Under the synthetic actions of continuous large coupler forces and track irregularities, the wheel of the middle wagon has a higher probability to climb onto the rail than the front and rear wagons. Under the effect of increasing coupler forces with constant yaw angle of 7 degrees, the wheel flange of the middle wagon approaches the rail and contacts it subsequently. The wheel flange cannot separate from the rail because of the strong constraints of drawbars and the continuous lateral forces applied by the drawbars. Under the excitation of the random irregularities, the wheel climbs onto the top of the railhead quickly, and then moves away from the rail. Based on the above analysis, it can be concluded that the simulation results are consistent with the field investigation results.

5. Parameter Influence on Derailment

To understand the effects of the coupler yaw angle, couple force, and wheel-rail friction coefficient on derailment, the values of the three parameters are assumed to vary. The simulation of parameter influence on derailment is conducted.

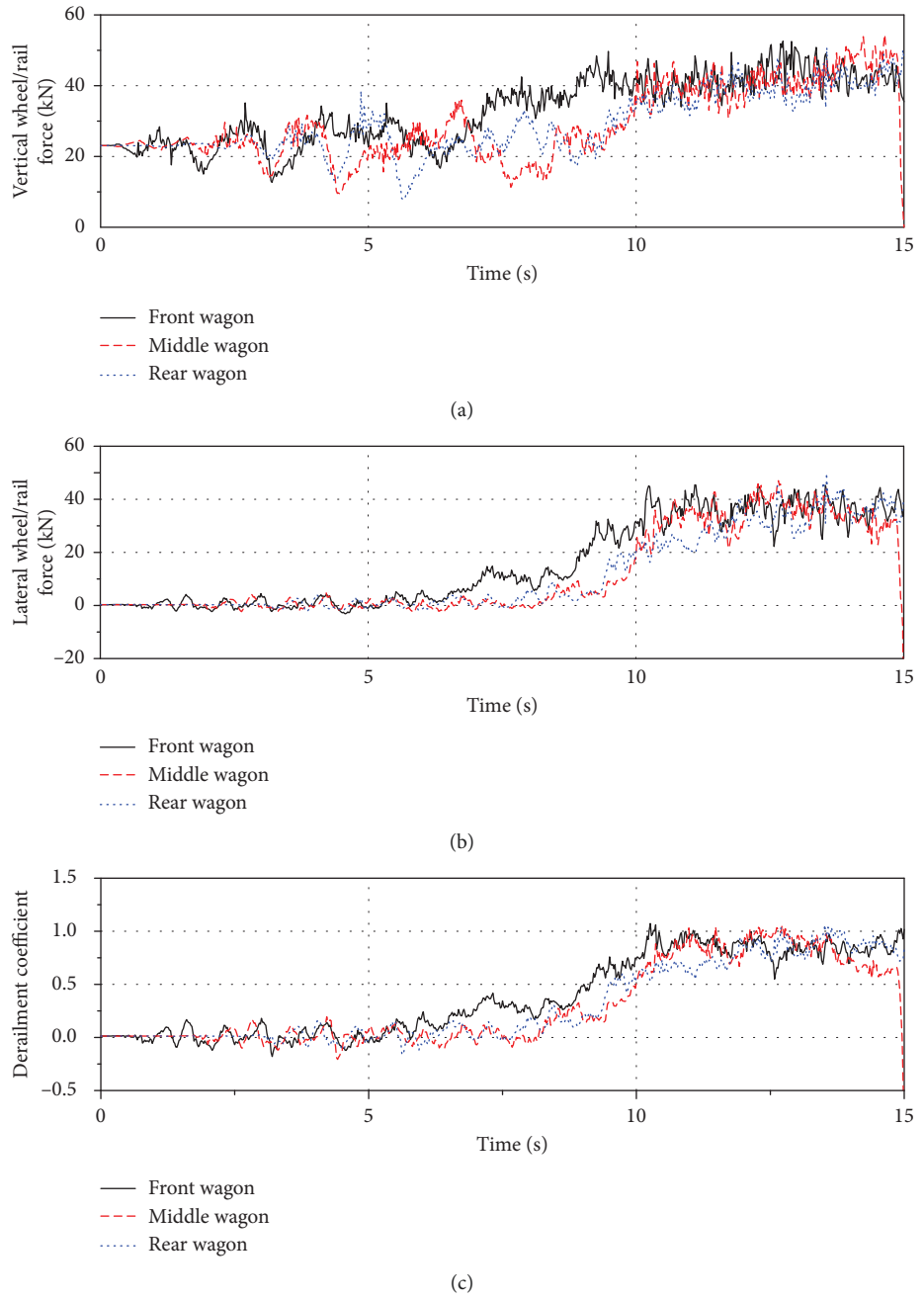

Figure 16: The comparison of dynamic performances: (a) vertical wheel/rail force; (b) lateral wheel/rail force; (c) derailment coefficient.

5.1. Coupler Yaw Angle. As the coupler yaw angle is hypothetical in the derailment simulation, it is significant to conduct further study on it. The coupler yaw angle is set to be 5, 6, 7, 8, and 9 degrees, meanwhile, the coupler force is set to increase linearly from 0 to 350 kN ($t = 5$~10 s) and keep constant ($t = 10$~15 s), and the wheel-rail friction coefficient is set to be 0.7.

Figure 17 shows the maximum derailment coefficient, wheel vertical rise, and lateral wheelset displacement under different coupler yaw angles. It should be noted that when the lateral wheelset displacements reach or exceed the critical value (54 mm), the maximums are recorded as 54 mm.

It can be seen from Figure 17(a) that the derailment coefficients of the 3-pack are less than 0.9 when the coupler yaw angle is 5 degrees. As the yaw angle reaches 6 degrees or above, the maximal derailment coefficients remain around 1.0. Figures 16(b) and 16(c) show that the lateral wheelset displacements and wheel vertical rises of the 3-pack are small when the coupler yaw angle is below 7 degrees. As the coupler yaw angle is set to be 7~8 degrees, the maximal lateral wheelset displacement of the middle wagon exceeds the limitation, while the displacements of the front and rear wagons are less than the critical value. Meanwhile, the maximal wheel vertical rises of the middle wagon reach

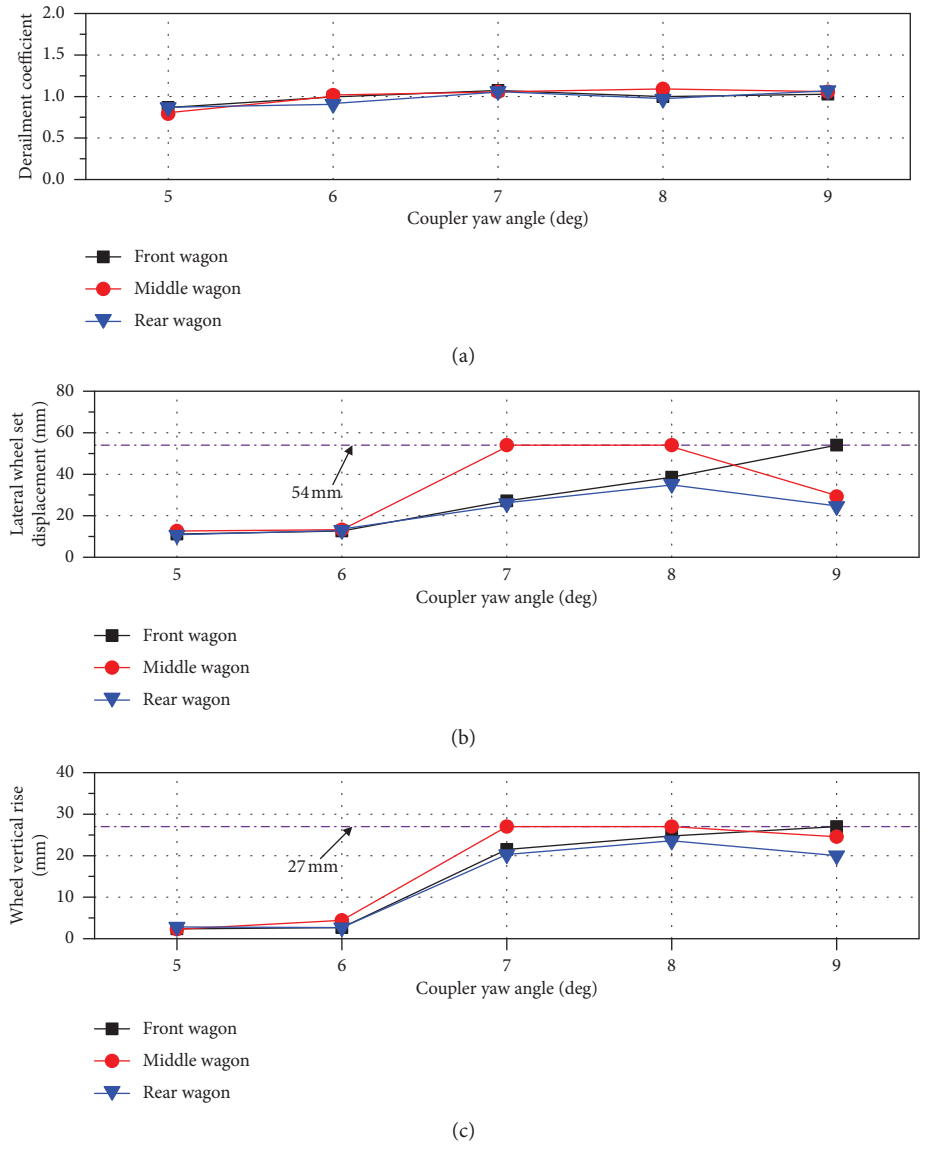

Figure 17: Effects of coupler yaw angle on (a) derailment coefficient, (b) lateral wheelset displacement, and (c) wheel vertical rise.

27 mm, and the wheel vertical rises of the front and rear wagons are 24.8 mm and 23.6 mm, respectively. It is indicated that the middle wagon has derailed. When the yaw angle is increased to 9 degrees, the lateral wheelset displacements of middle and rear wagons are below 30 mm, while the maximal lateral wheelset displacement of the front wagon exceeds the limitation. The maximal wheel vertical rise of all the wagons exceeds 20 mm, but only the wheel vertical rise of the middle wagon reaches the critical value. It means that the front wagon has derailed.

It is concluded that under 350 kN coupler force and 0.7 wheel-rail friction coefficient condition, increasing the coupler yaw angle will increase the risk of derailment. When the coupler yaw angle is between 7 and 8 degrees, the middle wagon of the 3-pack derails; however, the front wagon becomes the most dangerous one as the coupler yaw angle increases to 9 degrees.

5.2. Coupler Force. By longitudinal dynamics simulation, the coupler force of derailment simulation condition was determined; however, the actual coupler force during derailment remained to be unknown. To study the influence of coupler force on derailment, the coupler force is set to increase linearly from 0 to 250, 300, 350, 400, and 450 kN ($t = 5\sim10$ s), respectively, and keep constant ($t = 10\sim15$ s). Meanwhile, the coupler yaw angle is fixed at 7 degree, and the wheel-rail friction coefficient is set to be 0.7.

Figure 18 shows the maximum derailment coefficient, wheel vertical rise and lateral wheelset displacement, under different coupler force.

When the coupler force is set below 350 kN, the maximums of the derailment coefficient increase as the coupler forces increase and are less than 1.0. As the coupler force increases to 350 kN and above, the maximal derailment coefficients stay around 1.0, as shown in Figure 18(a). It is

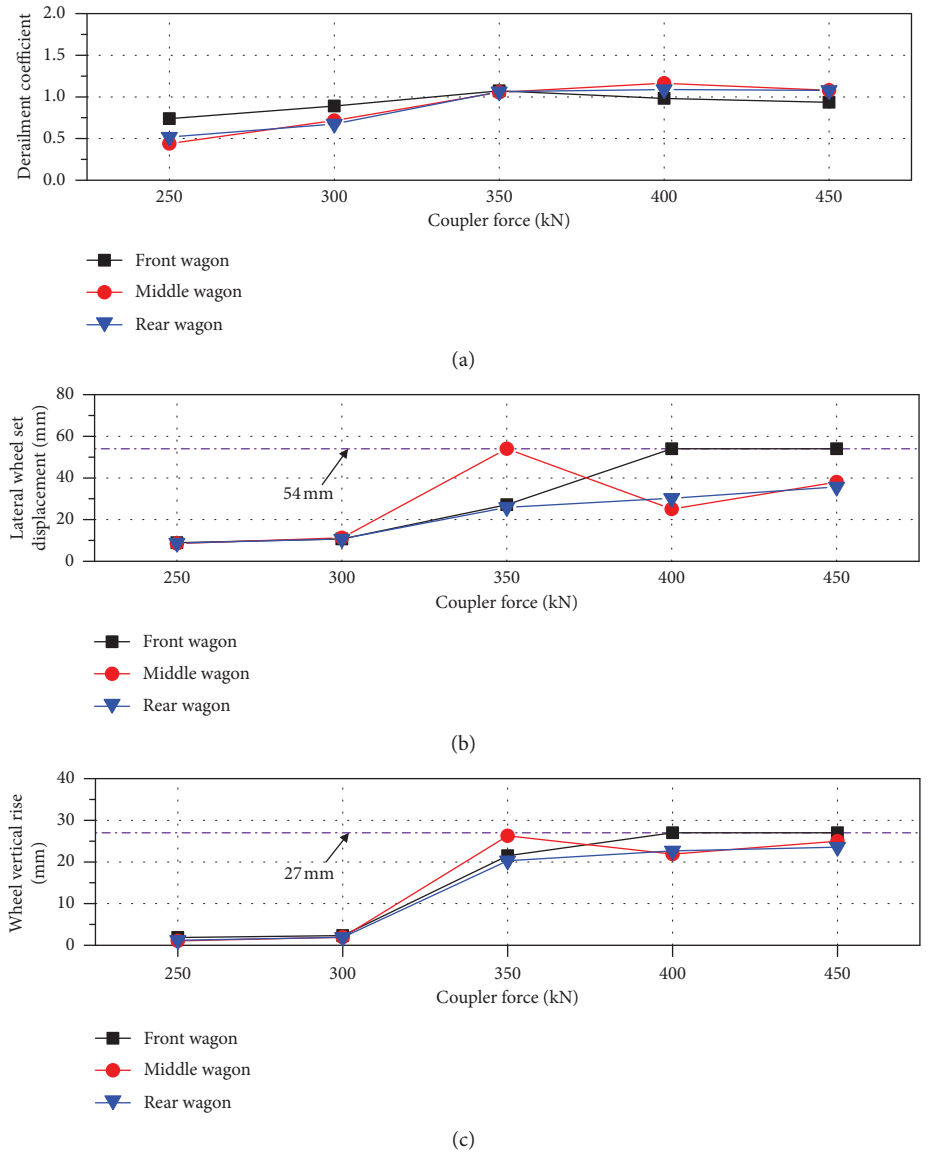

Figure 18: Effects of coupler force on (a) derailment coefficient, (b) lateral wheelset displacement, and (c) wheel vertical rise.

seen in Figures 18(b) and 18(c) that the lateral wheelset displacements and the wheel vertical rises are very small when the coupler forces are set to be 250 kN and 300 kN, which means low risks of derailment. When the coupler force is set to be 350 kN, the maximal lateral wheelset displacements of the front and rear wagons are about 27 mm, and the lateral wheelset displacement of the middle wagon exceeds the limitation. The maximal wheel vertical rise of the middle wagon reaches the critical value, while the wheel vertical rises of the front and rear wagons still stay in the allowable range. It can be judged that the middle wagon has derailed. As the coupler forces reach 400 kN and above, both the lateral wheelset displacement and wheel vertical rise of the front wagon reach the danger level, while the corresponding values of the middle and rear wagons are less than the critical values.

It can be concluded that under 7 degree coupler yaw angle and 0.7 wheel-rail friction coefficient condition, increasing the coupler force will increase the risk of derailment significantly. When the coupler force is kept below 300 kN, the risk of derailment is very small. When the coupler force is 320 kN, the middle wagon has a higher risk of derailment; however, the front wagon becomes the riskiest one when the coupler force reaches 400 kN and above.

5.3. Wheel-Rail Friction Coefficient. Considering the extreme situation, the wheel-rail friction coefficient of the 3-pack is set to vary from 0.1 to 0.9 with an interval of 0.1. The coupler force is set to increase linearly from 0 to 350 kN ($t = 5\sim10$ s) and keep constant ($t = 10\sim15$ s).

Figure 19 shows the maximums of the derailment coefficient, wheel vertical rise and lateral wheelset displacement under different wheel-rail friction coefficients.

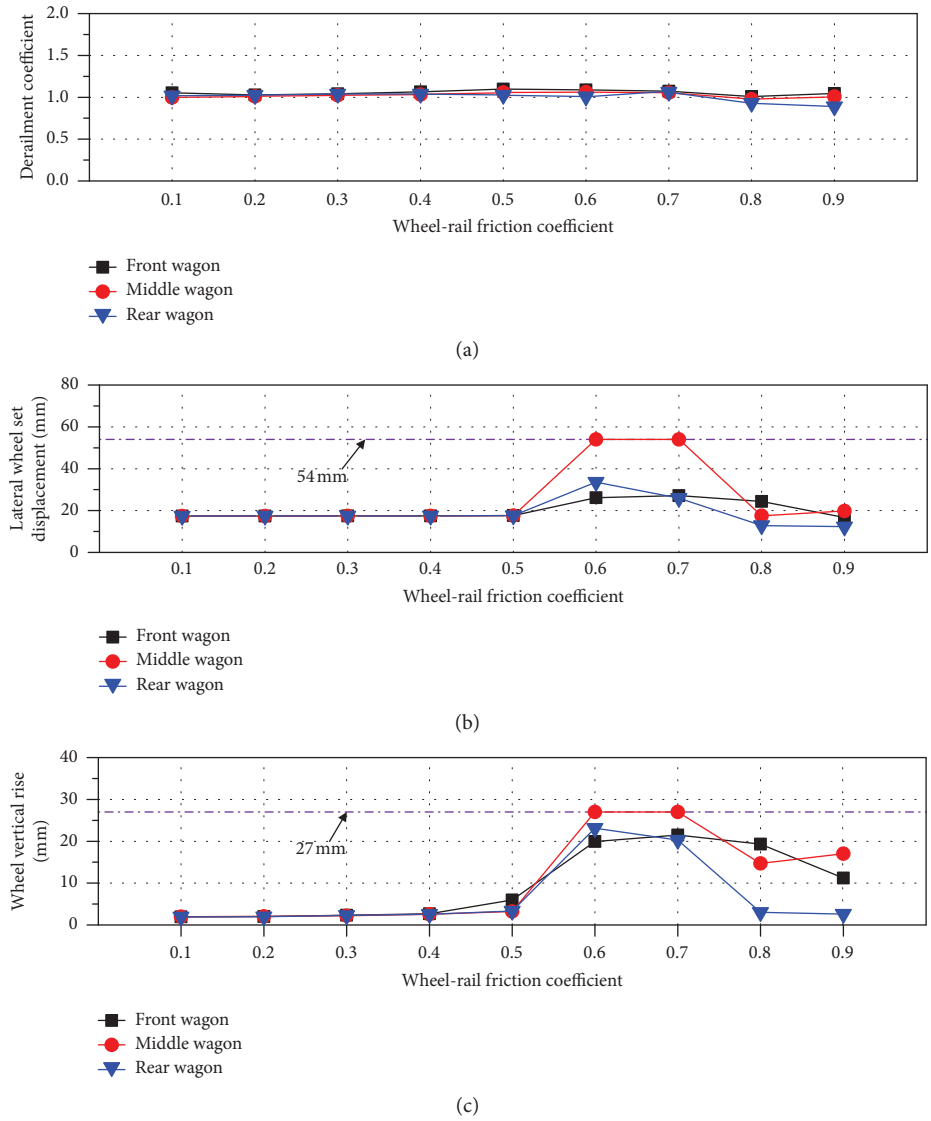

FIGURE 19: Effects of different wheel-rail friction coefficient on (a) derailment coefficient, (b) lateral wheelset displacement, and (c) wheelset vertical rise.

It is seen in Figure 19(a) that the maximal derailment coefficients of the 3-pack under the condition of different wheel-rail friction coefficients do not differ a lot, which stay around 1.0. Both the differences of the maximal lateral wheelset displacements and wheel vertical rises are small when $\mu \leq 0.5$. Figures 19(b) and 19(c) show that when μ is set to be 0.6 and 0.7, the maximal wheel vertical rises of all the three wagons exceed 20 mm, and the wheel vertical rises of the middle wagon reach the critical value. The maximal lateral wheelset displacements of the front and rear wagons are between 25 mm and 35 mm. Meanwhile, the lateral wheelset displacements of the middle wagon exceed the limitation, which means that the middle wagon has derailed. As μ exceeds 0.7, the maximal lateral wheelset displacements of the 3-pack decrease to below 25 mm. The maximal wheel vertical rises of the rear wagon are about 3 mm, while the corresponding values of the front and middle wagons are between 10 mm and 20 mm.

It can be concluded that under 350 kN coupler force with 7 degrees yaw angle, the wheel-rail friction coefficient affects the risk of derailment remarkably. When $\mu \leq 0.5$, the derailment risk is small because the rail cannot provide adequate climbing force. When μ is increased to 0.6~0.7, the rail applies a large tangential force on the wheel under the effect of large lateral coupler forces, which enables the wheel to climb onto the rail. Moreover, the constraints of the drawbars contribute to it a lot. When $\mu \geq 0.8$, the overlarge wheel-rail friction coefficient hinders the relative sliding between the wheel and rail, and the wheel cannot climb onto the rail. Hence, the lateral wheelset displacement and the wheel vertical rise are limited, and the derailment risk decreases. The large wheel-rail friction coefficient will exacerbate the wear of wheels and rails and reduce its service life. To balance the running safety and the service life, the friction coefficient should be controlled below 0.5, and the lubrication is proved to be an effective approach to control it [31, 32].

6. Conclusions

Aiming at an actual derailment accident, the influence factors of derailment of empty wagons are investigated. The 3-pack model composed of 3 C_{80}-type gondolas and two RFC-type drawbars is established. The field test results are adopted to validate the accuracy of the model. Based on the simulation model, the derailment process has been reconstructed, and the influence analysis of potential factors on derailment of empty wagons has been completed. The conclusions are drawn as follows:

(1) According to the field investigation results, the large coupler yaw angle and coupler force, the special connection mode by drawbars, and the poor conditions of wheel treads and flanges are supposed to be responsible for the accident.

(2) The simulation model is validated to simulate the dynamic braking on a straight track. The model can reflect the dynamic behaviour of the empty wagon during dynamic braking.

(3) Under the condition of 0.7 wheel-rail friction coefficient and 350 kN coupler forces with a coupler yaw angle of 7 degrees, the middle wagon of the 3-pack climbs onto the rail and moves forward for a short distance on the top of the railhead and derails subsequently, which is consistent with the field investigation results.

(4) The parameter influence analysis reveals that the coupler yaw angle, coupler force, and wheel-rail friction coefficient have significant influence on derailment. Increasing the coupler yaw angle and coupler force will increase the risk of derailment. Moreover, the derailed wagon will change from the middle wagon to the front one as the lateral component of the coupler force increases. When the friction coefficient is between 0.6 and 0.7, the middle wagon of the 3-pack derails, but the risk decreases as the friction coefficient reaches 0.8 and above.

(5) In order to enhance the running safety of the empty wagons, the wheel-rail friction coefficient should be no more than 0.5, as well as the operations of the train should be optimized to avoid an overlarge coupler yaw angle and a coupler force.

It should be noted that the above conclusions only have reference significance to the long freight train which is composed of the 3-pack units adopting drawbars.

Data Availability

The data that support the findings of this study include two parts, simulation results and test results. The simulation results were obtained from the simulation model. And, the models and the calculated conditions have been introduced clearly in the article. The test results were obtained from Dazhun Railway Company, which is our cooperative partner. But there are restrictions that apply to the availability of these measured data, which were used under license for the current study, and so are not publicly available.

Conflicts of Interest

The authors declare that they have no conflicts of interest.

Acknowledgments

The authors wish to express their thanks to State Key Laboratory of Traction Power for providing equipment and materials to this project and the China Dazhun Railway Company for the cooperation and support. The authors are grateful for the support by the National Natural Science Key Foundation of China (Grant nos. 51478399 and 51735012) and the Program of Introducing Talents of Discipline to Universities (111 Project) (Grant no. B16041).

References

[1] M. A. Britton, S. Asnaashari, and G. J. M. Read, "Analysis of train derailment cause and outcome in Victoria, Australia, between 2007 and 2013: implications for regulation," *Journal of Transportation Safety and Security*, vol. 9, no. 1, pp. 45–63, 2017.

[2] Q. Zeng, J. Xiang, and Z. Zhou, *Analysis Theory of Train Derailment and Its Application*, Central South University Press, Changsha, China, 2006.

[3] H. Weinstock, *Wheel Climb Derailment Criteria for Evaluation of Rail Vehicle Safety*, American Society of Mechanical Engineers, New York, NY, USA, 1984.

[4] N. Matsui, *Dynamics of High-Speed Rolling Stock*, Railway Technical Research Institute, Tokyo, Japan, 1966.

[5] W. Zhai, *Vehicle-Track Coupled Dynamics*, Science Press, Beijing, China, 4th edition, 2015.

[6] W. Zhai and G. Chen, "Method and criteria for evaluation of wheel derailment based on wheel vertical rise," *Journal of the China Railway Society*, vol. 23, no. 2, pp. 17–26, 2001.

[7] X. Jun and Z. Qingyuan, "A study on mechanical mechanism of train derailment and preventive measures for derailment," *Vehicle System Dynamics*, vol. 43, no. 2, pp. 121–147, 2005.

[8] K. Nagase, Y. Wakabayashi, and H. Sakahara, "A study of the phenomenon of wheel climb derailment: results of basic experiments using model bogies," *Proceedings of the Institution of Mechanical Engineers, Part F: Journal of Rail and Rapid Transit*, vol. 216, no. 4, pp. 237–247, 2002.

[9] J. Zeng and P. Wu, "Study on the wheel/rail interaction and derailment safety," *Wear*, vol. 265, no. 9-10, pp. 1452–1459, 2008.

[10] J. Zeng and Q. Guan, "Study on flange climb derailment criteria of a railway wheelset," *Vehicle System Dynamics*, vol. 46, no. 3, pp. 239–251, 2008.

[11] K. Wang, R. Zhang, Z. Chen et al., "Effect of coupler position errors on dynamic performance of heavy haul locomotive," *Journal of Southwest Jiaotong University*, vol. 50, no. 6, pp. 1041–1046, 2016.

[12] Z. Shi, K. Wang, L. Guo, Z. Chen, R. Zhang, and K. Lv, "Effect of arc surfaces friction coefficient on coupler stability in heavy haul locomotives: simulation and experiment," *Vehicle System Dynamics*, vol. 55, no. 9, pp. 1368–1383, 2017.

[13] K. Lv, K. Wang, Z. Chen et al., "The effect of the secondary lateral stopper on the compressed stability of the couplers and running safety of the locomotives," *Proceedings of the Institution of Mechanical Engineers, Part F: Journal of Rail and Rapid Transit*, vol. 232, no. 3, pp. 851–862, 2018.

[14] Z. Xu, W. Ma, Q. Wu, and S. H. Luo, "Coupler rotation behaviour and its effect on heavy haul trains," *Vehicle System Dynamics*, vol. 51, no. 12, pp. 1818–1838, 2013.
[15] L. Guo, K. Wang, Z. Chen, Z. Shi, K. Lv, and T. Ji, "Analysis of the car body stability performance after coupler jack-knifing during braking," *Vehicle System Dynamics*, vol. 56, no. 6, pp. 900–922, 2017.
[16] C. Cole and Y. Sun, "Simulated comparisons of wagon coupler systems in heavy haul trains," *Proceedings of the Institution of Mechanical Engineers, Part F: Journal of Rail and Rapid Transit*, vol. 220, no. 3, pp. 247–256, 2006.
[17] Q. Wu, M. Spiryagin, and C. Cole, "Advanced dynamic modelling for friction draft gears," *Vehicle System Dynamics*, vol. 53, no. 4, pp. 475–492, 2015.
[18] C. Cole, M. Spiryagin, Q. Wu, and Y. Q. Sun, "Modelling, simulation and applications of longitudinal train dynamics," *Vehicle System Dynamics*, vol. 55, no. 10, pp. 1498–1571, 2017.
[19] M. Durali and B. Shadmehri, "Nonlinear analysis of train derailment in severe braking," *Journal of Dynamic Systems, Measurement, And Control*, vol. 125, no. 1, pp. 48–53, 2003.
[20] C. Hung, Y. Suda, M. Aki et al., "Study on detection of the early signs of derailment for railway vehicles," *Vehicle System Dynamics*, vol. 48, no. 1, pp. 451–466, 2010.
[21] L. Guo, K. Wang, J. Lin et al., "Study of the post-derailment safety measures on low-speed derailment tests," *Vehicle System Dynamics*, vol. 54, no. 7, pp. 943–962, 2016.
[22] X. Wu, M. Chi, H. Gao et al., "The study of post-derailment measures to limit the extent of a derailment," *Proceedings of the Institution of Mechanical Engineers, Part F: Journal of Rail and Rapid Transit*, vol. 230, no. 1, pp. 64–76, 2016.
[23] S. Iwnicki, *Handbook of Railway Vehicle Dynamics*, CRC Press, Boca Raton, FL, USA, 2006.
[24] F. J. Nadal, *Theorie de la Stabilite des Locomotives*, Vve C. Dunod et P. Vicq, Paris, France, 1896.
[25] P. Liu, W. Zhai, and K. Wang, "Establishment and verification of three-dimensional dynamic model for heavy-haul train–track coupled system," *Vehicle System Dynamics*, vol. 54, no. 11, pp. 1511–1537, 2016.
[26] Y. Huang, F. Li, M. Fu et al., "Comparison of algorithms for discontinuity on the characteristics curves of draft gears," *Journal of Southwest Jiaotong University*, vol. 40, no. 1, pp. 9–12, 2005.
[27] Q. Xiao, C. Wang, X. Zhou et al., "Analysis on the characteristics of wheel/rail rolling contact under different friction coefficient," *China Railway Science*, vol. 32, no. 4, pp. 66–71, 2011.
[28] H. H. Koci and C. A. Swenson, "Locomotive wheel-rail loading-a systems approach," in *Proceedings of Heavy Haul Railways Conference*, p, 365, Institution of Engineers, Perth, Australia, September 1978.
[29] W. C. Shust, R. Thompson, and J. Elkins, "Controlled wheel climb derailment tests using a force measuring wheelset and AAR's track loading vehicle," in *Proceedings of 12th International Wheelset Congress*, Qingdao, China, September 1998.
[30] M. Durali and M. M. Jalili, "A new criterion for assessment of train derailment risk," *Proceedings of the Institution of Mechanical Engineers, Part K: Journal of Multi-body Dynamics*, vol. 224, no. 1, pp. 83–101, 2010.
[31] M. Tomeoka, N. Kabe, M. Tanimoto, E. Miyauchi, and M. Nakata, "Friction control between wheel and rail by means of on-board lubrication," *Wear*, vol. 253, no. 1-2, pp. 124–129, 2002.
[32] M. Ishida, T. Ban, K. Iida, H. Ishida, and F. Aoki, "Effect of moderating friction of wheel/rail interface on vehicle/track dynamic behavior," *Wear*, vol. 265, no. 9-10, pp. 1497–1503, 2008.